A data-driven model for constraint of present-day glacial isostatic adjustment in North America

Simon, K. M.; Riva, R. E.M.; Kleinherenbrink, M.; Tangdamrongsub, N.

DOI
10.1016/j.epsl.2017.06.046

Publication date
2017

Document Version
Accepted author manuscript

Published in
Earth and Planetary Science Letters

A data-driven model for constraint of present-day glacial isostatic adjustment in North America

K.M. Simon[1*], R.E.M. Riva[1], M. Kleinherenbrink[1], and N. Tangdamrongsub[1,2]

[1]Delft University of Technology, Department of Geoscience and Remote Sensing, Stevinweg 1, 2628 CN Delft, the Netherlands
[2]University of Newcastle, School of Engineering, Faculty of Engineering and Built Environment, Callaghan, New South Wales, Australia

*Corresponding author: +31 15 2788147, k.m.simon@tudelft.nl

Abstract

Geodetic measurements of vertical land motion and gravity change are incorporated into an *a priori* model of present-day glacial isostatic adjustment (GIA) in North America via least-squares adjustment. The result is an updated GIA model wherein the final predicted signal is informed by both observational data, and prior knowledge (or intuition) of GIA inferred from models. The data-driven method allows calculation of the uncertainties of predicted GIA fields, and thus offers a significant advantage over predictions from purely forward GIA models. In order to assess the influence each dataset has on the final GIA prediction, the vertical land motion and GRACE-measured gravity data are incorporated into the model first independently (i.e., one dataset only), then simultaneously. The relative weighting of the datasets and the prior input is iteratively determined by variance component estimation in order to achieve the most statistically appropriate fit to the data. The best-fit model is obtained when both datasets are inverted and gives respective RMS misfits to the GPS and GRACE data of 1.3 mm/yr and 0.8 mm/yr equivalent water layer change. Non-GIA signals (e.g., hydrology) are removed from the datasets prior to inversion. The post-fit residuals between the model predictions and the vertical motion and gravity datasets, however, suggest particular regions where significant non-GIA signals may still be present in the data, including unmodelled hydrological changes in the central Prairies west of Lake Winnipeg. Outside of these regions of misfit, the posterior uncertainty of the predicted model provides a measure of the formal uncertainty associated with the GIA process; results indicate that this quantity is sensitive to the uncertainty and spatial distribution of the input data as well as that of the prior model information. In the study area, the predicted uncertainty of the present-day GIA signal ranges from ~0.2-1.2 mm/yr for rates of vertical land motion, and from ~3-4 mm/yr of equivalent water layer change for gravity variations.

Keywords: Glacial isostatic adjustment, GRACE, GPS, North America

1. Introduction and Previous Modelling Studies

Glacial isostatic adjustment (GIA) is the Earth's ongoing long-term (kyr-scale) viscoelastic response to surface loading and unloading by the ice sheets that existed during past glacial cycles. GIA causes deformation of the Earth's solid surface and gravitational potential field, and these deformations in turn result in sea-level changes via the redistribution of water in the global ocean (e.g., Peltier 1974, Farrell and Clark 1976, Peltier and Andrews 1976, Clark et al. 1978, Mitrovica and Peltier 1991). The absolute magnitude of the long-term GIA contribution to present-day observables (crustal deformation, gravity field perturbations, sea-level change) is largest in regions proximal to the former ice sheets. However, at all locations on the globe, ongoing GIA from the last glacial cycle can represent a significant fraction of the total value of observed present-day change. Consequently, constraining the contribution of shorter time-scale processes (contemporary ice mass loss, continental hydrology variations, oceanographic changes) to total present-day rates of crustal deformation, gravity change, and sea-level variation, requires an estimate of the GIA response at present day (e.g., Peltier and Tushingham 1989, Tamisiea and Mitrovica 2011).

Because glacial isostatic adjustment can seldom be measured directly, the present-day GIA response is often estimated by forward models (e.g., Lambeck et al. 1998, Peltier 2004, Spada et al. 2006, Peltier et al. 2015). Forward modelled GIA is sensitive to several poorly constrained variables, including ice sheet history, elastic lithospheric thickness, the magnitude and parameterization of mantle viscosity, and the effects of lateral changes in Earth structure (e.g., Tushingham and Peltier, 1991, Lambeck et al. 1998, Latychev et al. 2005, van der Wal et al. 2010, Tamisiea 2011, Peltier et al. 2015), although forward model predictions typically lack any formal quantification of the uncertainties associated with the input model combinations. However, variation of input model parameters within a reasonable range of values can result in significant changes to the magnitude (and sometimes the sign) of the predicted GIA response, indicating GIA uncertainty is large. This observation holds even in far-field regions, which are characterized by much smaller GIA signals than near-field regions. For example, Mitrovica and Davis (1995) found that estimates of the GIA contribution to far-field sea-level change varied by as much as ~0.3-0.5 mm/yr for a range of GIA models, a value which represents

~10-20% uncertainty in the GIA contribution relative to their mean total far-field sea-level rate estimated from tide gauge measurements (~1.4 mm/yr).

As datasets from satellite geodesy missions have increased both in quantity and duration of observation, increasing emphasis has been placed on the use of data-driven methods to constrain better the individual components of total measured present-day change rates (Riva et al. 2009, Hill et al. 2010, Wu et al. 2010a, Rietbroek et al. 2012, Sasgen et al. 2012, Lambert et al. 2013, Wang et al. 2013, Zhao 2013, Gunter et al. 2014, Wang et al. 2015). A main limitation of these types of models is that they typically focus on present-day GIA signals, and therefore offer little insight into the time-varying GIA response or ice sheet evolution. However, while the method, study area, and quantity of primary interest vary by study, all of these studies either eliminate or reduce the uncertainty associated with forward modelled GIA (through the use of separation approaches, or data-driven inversion approaches, respectively).

In North America, separation approaches that use a combination of GPS measurements and observations from the Gravity Recovery and Climate Experiment (GRACE) have been employed to estimate recent continental hydrology changes (Lambert et al. 2013, Wang et al. 2013, 2015). Although Lambert et al. (2013) and Wang et al. (2013, 2015) use different methodologies, both methods assume a relationship between GIA-induced changes to vertical land motion and gravity change that can be used to separate and remove the GIA effect from total measured rates (e.g., Wahr et al. 1995), and thus avoid the use of forward modelled GIA predictions. Data-model combination approaches involving the simultaneous adjustment of geodetic measurements with *a priori* forward modelled GIA information have been applied globally (Wu et al. 2010a), in North America (Sasgen et al. 2012, Zhao 2013), Antarctica (Sasgen et al. 2013), and Fennoscandia (Hill et al. 2010). These data combination approaches yield updated models of present-day GIA informed by both observational data and prior expectation of GIA motions derived from models, although in the North American studies, the focus was not placed on quantifying GIA uncertainty. The methodology of Hill et al. (2010) was also used to obtain the GIA model used for the Stable North American Reference Frame (SNARF) (https://www.unavco.org/projects/past-projects/snarf/snarf.html).

In this study, we extend the data-driven combination method of Hill et al. (2010) to obtain a prediction of present-day GIA in North America. Relative to the SNARF project, which used a similar methodology, we include GRACE data, as well as use updated vertical land motion data and an updated North American ice sheet reconstruction to generate the prior GIA information. We also use variance component estimation to weight the contributions of the data and prior input to the final model prediction. Our goal is to obtain a present-day GIA solution for the study region that adequately predicts available observational constraints, minimizes the uncertainty associated with the forward modelled GIA inputs, and includes a realistic estimation of formal model error.

2. Methodology

The GIA response is solved for by least-squares adjustment, following the methods described by Hill et al. (2010). The final predicted GIA model response is represented by vector m^*, where the response represents the GIA-related deformation type(s) of interest. Here, the predicted deformation types are rates of vertical crustal motion and gravity change. A solution for m^* is obtained by minimizing the objective function of the data misfits and the *a priori* model misfits (e.g., Tarantola 2005)

$$\varphi(m^*) = (d - A \cdot m^*)^T {C_d}^{-1}(d - A \cdot m^*) + (m^* - m)^T {C_m}^{-1}(m^* - m), \qquad (2.1)$$

where d is a vector of GIA-induced observations, A is the design matrix, C_d is the data covariance matrix, m is a vector of *a priori* GIA predictions, and C_m is the prior model covariance matrix.

2.1 Observational Inputs

The observation vector d contains N measurements of GIA-related observations. In this study, depending on the combination of data that is inverted, d contains observed vertical land motion rates, GRACE-measured gravity change rates, or both. N is the total number of input observations used to constrain the solution. For example, if n_{GPS} vertical land motion data and n_{GRACE} GRACE data points are inverted simultaneously, then $N = n_{GPS} + n_{GRACE}$. The data covariance matrix C_d is an $N \times N$

matrix containing the covariances associated with the observations. The component of C_d associated with the vertical land motion data is assumed to be diagonal (variances only), while the component of C_d associated with the GRACE gravity data includes the full covariance matrix of the trend. The data are described further in Sections 3.1-3.3.

2.2 Model Inputs

The *a priori* model vector m contains the mean of a suite of forward-modelled GIA predictions. Each model deformation type is predicted at each of the input observation sites, as well as on a grid of the study area. The length of vector m is thus the sum of the total number of predictions at observation sites and the total number of predictions at grid locations, or $M = M_{obs} + M_{grid}$. For two model deformation quantities (vertical motion and gravity change) and a grid of n_{grid} locations, $M_{grid} = 2n_{grid}$ and $M_{obs} = 2N$.

There are no formal uncertainties associated with forward GIA models. However, for a suite of GIA models that spans a reasonable range of parameter space, an input model covariance matrix can be constructed using

$$C_m^{ij} = \frac{1}{\Omega}\sum_{k=1}^{\Omega}\left(m_i^k - m_i\right)\left(m_j^k - m_j\right) \quad i,j = 1,\ldots,M, \tag{2.2}$$

where $k = 1,\ldots,\Omega$ represents the suite of Ω forward models, m_i^k is the model prediction at the i^{th} spatial location in the k^{th} GIA model, m_i is the average prediction of Ω models at the i^{th} location, and here *i* and *j* are the indices of the model covariance matrix. The *a priori* model averages and the associated suite of GIA model predictions are discussed further in Section 3.4.

2.3 Design Matrix

The *N* × *M* design matrix *A* consists of the partial derivatives of the observations with respect to the model parameters according to

$$A_{ij} = \left.\frac{\partial d_i}{\partial m_j^*}\right|_{m^*=m} \qquad i = 1, \cdots, N;\ j = 1, \cdots, M. \tag{2.3}$$

If the location of the *i*th observation coincides with the location of the *j*th model prediction, and the observation type is equal to the model prediction deformation type, then the design matrix has a value of 1. The design matrix has a value of 0 at all other locations (that is, all locations in *i* and *j* where the site location and deformation type are not coincident). In this study, the deformation type is either vertical motion or gravity change.

2.4 Model Solution

Minimizing the objective function in equation 2.1 with respect to the model solution by setting $\frac{\partial \varphi}{\partial m^*} = 0$ yields the model solution (e.g., Tarantola 2005)

$$m^* = m + (A^T C_d^{-1} A + C_m^{-1})^{-1} A^T C_d^{-1}(d - Am), \tag{2.4}$$

with a posterior covariance matrix of

$$C_{m^*} = (A^T C_d^{-1} A + C_m^{-1})^{-1}. \tag{2.5}$$

Both the GPS and GRACE datasets are incorporated into the model solution together, as well as independently, for a total of three scenarios. Each dataset is weighted relative to the prior information (and in the case of the combined solution, relative to each other) using variance component estimation (VCE) following the description of Koch and Kusche (2002). When weighting is applied to the solution, equation 2.4 takes the form

$$m^* = m + \left(\frac{1}{\sigma_d^2} A^T C_d^{-1} A + \frac{1}{\sigma_\lambda^2} C_m^{-1}\right)^{-1} A^T \frac{1}{\sigma_d^2} C_d^{-1}(d - Am) \tag{2.6}$$

where σ_d^2 is the variance factor applied to the data and σ_λ^2 is the variance factor applied to the prior. If both datasets are incorporated into the model solution, then each dataset has its own variance factor. The influence of the prior model on the model solution is inversely proportional to the variance factor, σ_λ^2; that is, the influence of the prior information decreases as σ_λ^2 increases. Further discussion of the variance component estimation is found in Section 4.3 and the supplementary material.

3. Observational Data and Model Inputs

3.1 Vertical Land Motion Data

Rates of vertical land motion are obtained from the solution in the supplementary material of Peltier et al. (2015). Only rates from within the North American study area are selected. Peltier et al. (2015) did not include sites from westernmost North America in their supplement, possibly due to the potentially significant contribution to the measured rate from tectonic deformation. Several studies have for example suggested that in addition to GIA, west coast sea-level data may include signals from tectonic deformation (e.g., Clague et al. 1982, James et al. 2009a, Roy and Peltier 2015) and that regional GIA models may require decreased upper mantle viscosity values to best fit sea-level data there (e.g., James et al. 2009b). Therefore, to avoid the influence of active tectonics, and similar to other studies (Sella et al. 2007), GPS data from the western part of the continent are excluded here. We also exclude locations where there may be contributions to vertical motion from present-day mass loss of glaciers and ice caps (Alaska, and islands within the Canadian Arctic Archipelago) (Arendt et al. 2002, Gardner et al. 2011, Jacob et al. 2012), and sedimentation and subsurface fluid withdrawal (Gulf of Mexico coastline) (Ivins et al. 2007, Kolker et al. 2011, Letetrel et al. 2015). 340 measurements comprise the dataset of vertical land motion rates (Figure 1). We additionally remove the effect of hydrological loading from the vertical velocities (Section 3.3).

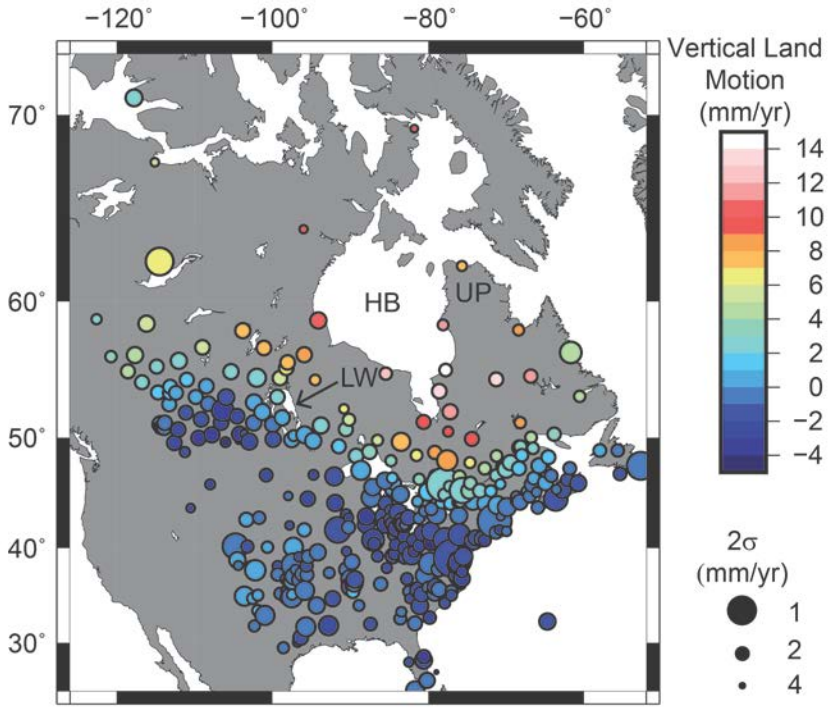

Figure 1. Vertical land motion rates in North America used as input for the inversion, from the solution of Peltier et al. (2015). Measurements from sites significantly influenced by non-GIA processes are removed, as discussed in Section 3.1. Uncertainties are shown as 95% confidence limits (2σ); symbol size is inversely proportional to uncertainty size. HB – Hudson Bay, LW – Lake Winnipeg, UP – Ungava Peninsula.

The vertical motion data consist primarily of measurements from continuous GPS sites, as well as rates from Canadian Base Network (CBN) episodic GPS sites, although a limited number (<5%) of velocities are also estimated using VLBI, SLR and DORIS observations (Peltier et al. 2015). The continuous GPS data span a time period from 1994 to 2012, with the lengths of the individual time series ranging from approximately 4 to 16 years, while the episodic CBN rates are derived from four occupations between 1996 and 2011. The data are aligned in the International GNSS Service (IGS) reference frame IGS08, which is a realization of the International Terrestrial Reference Frame solution ITRF2008 (Altamimi et al. 2011). The vertical velocities are represented in the centre of mass (CM) frame. The data processing for the vertical motion solution is discussed further in Peltier et al. (2015) and Argus et al. (2014). In Peltier et al. (2015), the uncertainties of the vertical motion rates are expressed as 95% confidence limits (2σ). The input data covariance matrix C_d of the vertical motion measurements is represented by a diagonal matrix of the associated variances (σ^2).

3.2 GRACE Data

Gravity change rates are estimated using GRACE Release-05 (RL05) monthly solutions from the University of Texas at Austin Center for Space Research (CSR). The coefficients are truncated at degree and order 96, consistent with a spatial resolution of ~200 km. The C_{20} coefficients are replaced with values estimated from Satellite Laser Ranging (Cheng et al. 2013). The GRACE data are naturally in the CM frame, thus degree 1 coefficients are not necessary. The monthly fields are filtered with a statistically optimal Wiener filter following Klees et al. (2008). The optimal filter incorporates the full variance-covariance information of the monthly solutions, and is designed to filter less aggressively in regions where signal is stronger (e.g., over regions with a significant hydrological cycle). Using 113 monthly solutions that span a time period of ~10.5 years (2004.02 to 2014.06), a mass trend is estimated that accounts for bias, as well as annual and semi-annual variations. The estimated mass trend incorporates the full error covariance matrices of the monthly solutions, and the covariance of the resulting trend coefficients is represented by the full covariance matrix of the linear parameter estimate. The trend uncertainties thus differ from the more zonal patterns estimated by filters that do not include information about the signal and noise covariances. The trend coefficients and the associated covariance terms are represented on a uniform 2° × 2° grid over North America.

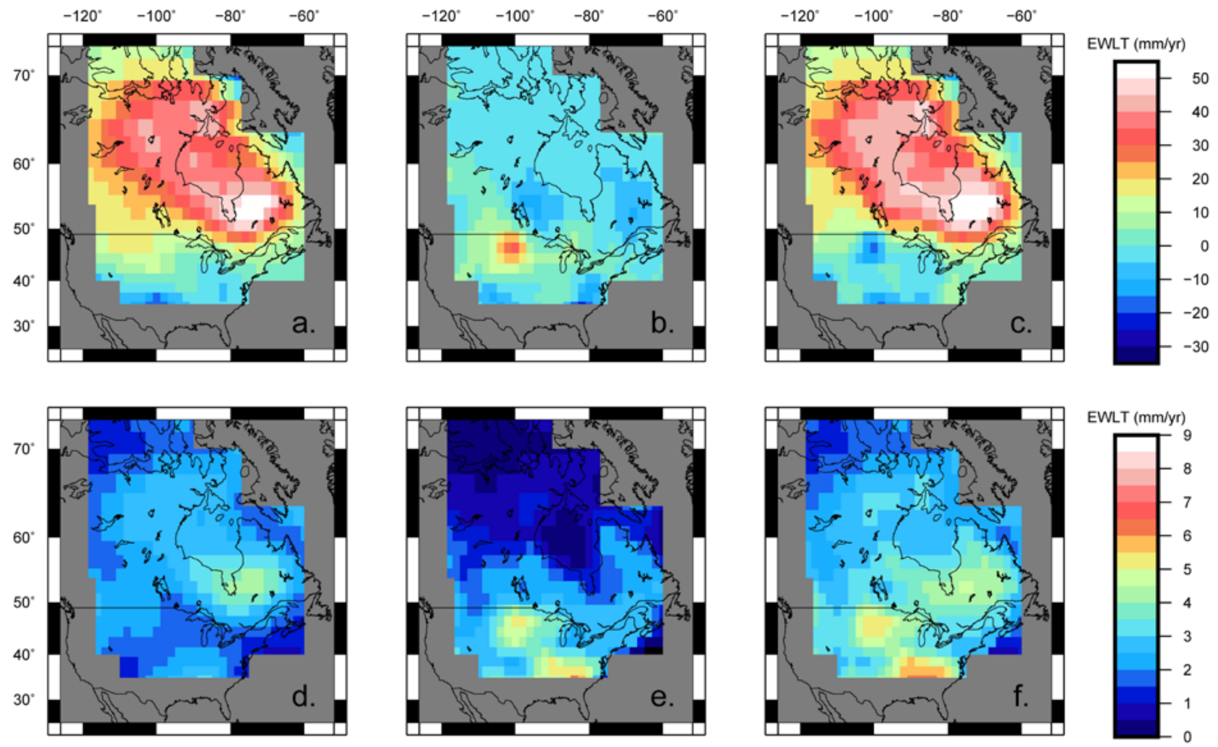

Figure 2. GRACE mass trend, uncorrected for hydrology changes (a), hydrology changes derived from model PCR-GLOBWB (b), GRACE mass trend corrected for hydrology (c). (d)-(f): The 2σ uncertainty associated with each of (a)-(c). Time span of all trends is 2004.02 – 2014.06. Units are mm/yr of change to equivalent water layer thickness (EWLT).

As with the vertical motion data, the gravity signal over North America is not everywhere dominated by the long-term GIA response that we wish to model. Some regions are significantly influenced by non-GIA effects, such as present-day mass loss of glaciers and ice caps, and thus these locations are not included in the input dataset. The final dataset for the study area consists of 468 gravity change estimates on a grid over North America, and a full covariance matrix, C_d. The derived gravity trend and its associated uncertainty are shown in Figures 2a,d. The total gravity trend is corrected for changes in terrestrial water storage as described in the next section (3.3).

3.3 Hydrology Correction for GRACE and GPS Data

We estimate terrestrial water storage changes using the global hydrology model PCRaster Global Water Balance (PCR-GLOBWB) (Wada et al. 2010, 2014). In the supplementary material, it is shown that the results are not strongly sensitive to the choice of hydrology model, but that including a correction for hydrology can yield a slightly improved result overall. In PCR-GLOBWB, the total water storage is the sum of five contributions: groundwater, snow, soil moisture, surface water, and other processes (canopy interception, irrigation, and river channels). The model predictions are expressed as averaged monthly model solutions on a 0.5° × 0.5° global grid. Using the same methodology and time span as was used with the GRACE data, we fit a trend to the monthly model predictions. In order to use the same spatial resolution as the GRACE data, the gridded trend prediction is transformed into a spherical harmonic expansion truncated at degree and order 96. A fan filter with maximum degree 96 is then applied to the trend coefficients in order to suppress ringing artefacts (e.g., Siemes et al. 2013, Zhang et al. 2009). The degree 1 component was not removed from the hydrological signal at this stage, but we find that its inclusion has only a small effect on the computed trend (in fact, inclusion of the hydrological correction itself has only a small impact on the results). Finally, the trend coefficients are transformed back to the spatial domain onto a 2° × 2° grid and removed from the total GRACE-derived gravity trend (Figure 2c). The uncertainties in the hydrological signal are estimated as the uncertainty in the linear parameter estimate (Figure 2e); the GRACE uncertainties and the hydrological uncertainties are added in quadrature for the total corrected signal (Figure 2f).

The vertical motion data are also corrected for the effect of hydrological loading. The vertical elastic response associated with the hydrology trend derived from PCR-GLOBWB is estimated using elastic Earth parameters averaged from the Preliminary Reference Earth Model (Dziewonksi and Anderson 1981), and then removed from the total measured vertical land motion rates prior to the inversion. Within the study area, the model-predicted effect of hydrological loading on vertical velocities is generally small (on average, less than 0.2 mm/yr), and is less than the 1σ uncertainty of the observations at all sites.

3.4 Prior GIA Models

The *a priori* GIA model (m in equation 2.4) consists of predictions of present-day vertical land motion change and gravity change, and is the average of multiple predictions from a suite of GIA models that varies the Earth's rheological structure and ice sheet history. In total, 150 model combinations are used (75 Earth models and 2 ice sheet histories). The Earth models have a 90 km thick elastic lithosphere and an underlying 2-layer compressible viscoelastic mantle. The upper mantle (>660 km depth) viscosity values span 1×10^{19} Pa s – 5×10^{21} Pa s, and the lower mantle viscosity values span 1×10^{20} Pa s – 1×10^{23} Pa s. Consistent with the data constraints, the deformations of the GIA models are calculated in the CM frame.

The first ice sheet scenario uses the SJD15 and Laur16 models for the Innuitian and Laurentide ice sheets, respectively (Simon et al. 2015, 2016). These models feature a North American ice sheet complex that has been modified relative to the global ICE-5G model (Peltier 2004) to provide an improved fit of GIA model predictions to relative sea-level measurements and GPS-measured vertical land motions in north-central Canada; ICE-5G is used for the rest of the globe in this version of the ice sheet history. The second ice sheet scenario uses the global ICE-5G reconstruction of Peltier (2004). The North American ice thickness history of ICE-5G differs significantly from Laur16 and SJD15. In particular, relative to ICE-5G, Laur16's ice cover is thinner west of Hudson Bay by ~30%, and thicker east of Hudson Bay by ~20-25%. These modifications to the North American component of ICE-5G address ICE-5G's significant overprediction and underprediction of vertical land motion and gravity rates west and east of Hudson Bay, respectively (e.g., Lambert et al. 2006, Argus and Peltier 2010, Peltier et al. 2015).

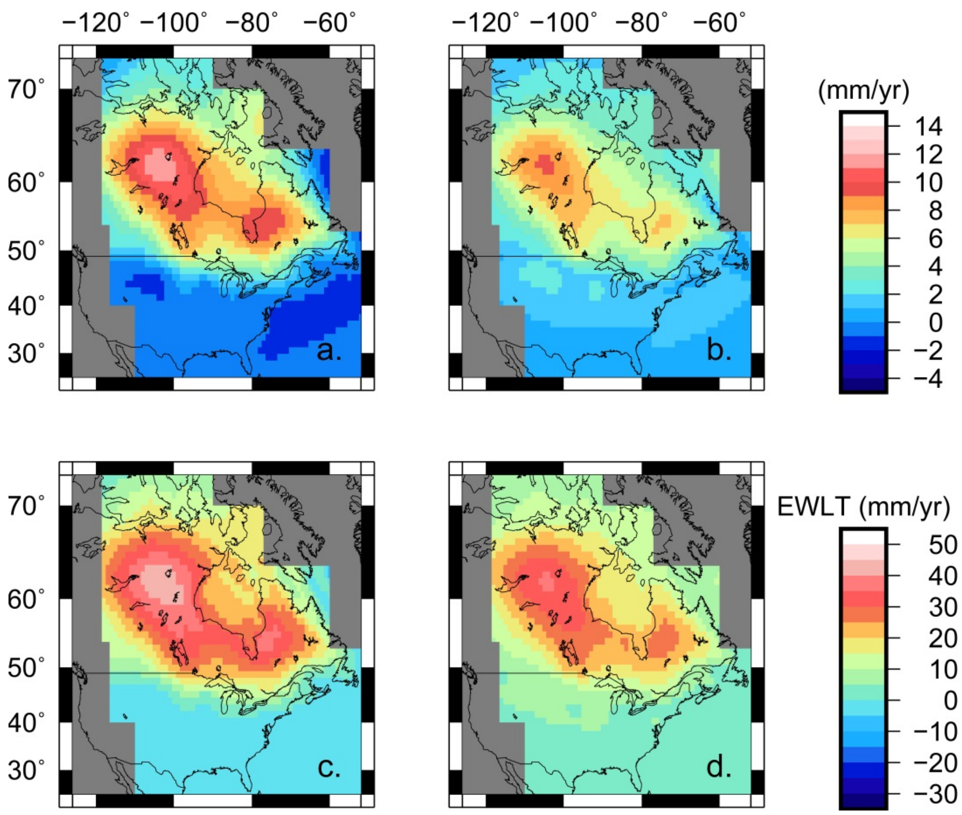

Figure 3. *A priori* GIA model inputs. Shown are vertical land motion rates averaged over a suite of 150 models (a) and the associated standard deviation of the vertical motion rates for the entire suite of models (b). (c) and (d) are the same as (a) and (b), except rates of gravity change are shown and are expressed as change to equivalent water layer thickness (EWLT). Uncertainty rates are not VCE-scaled.

The input model covariance matrix for the suite of GIA models is constructed using equation 2.2 with small perturbations added to the main diagonal to yield a full-ranked matrix. Figure 3 shows the averaged *a priori* model predictions $\langle m_i \rangle$ and their associated uncertainty (i.e., $\sqrt{C_m^{ii}}$). The averaged predicted rates display characteristics of both ICE-5G and Laur16. For instance, west and east of Hudson Bay, two distinct domes of vertical uplift are clearly visible (Laur16), with the largest averaged rates present to the west of Hudson Bay (ICE-5G) (Figure 3). The regions with the largest ice load also have the largest uncertainty rates, consistent with the results of Wu et al. (2010b). The use of 75 Earth models and 2 different ice load histories allows the final model prediction to vary both as a function of mantle viscosity and ice thickness. The sensitivity of the final model prediction to variations in the *a* *priori* information is examined in the supplementary material (Section S2). Characteristic behaviours and misfits of selected models from the *a priori* set are also examined in the supplement (Section S4).

4. Results

The data are inverted simultaneously with the *a priori* information for the present-day GIA response (equation 2.8). We discuss the prediction of both model deformation types (vertical land motion and gravity change) for three scenarios: i) inversion of only the vertical motion data (termed 'Data-driven 1', or D1), ii) inversion of only the gravity change data (D2), and iii) inversion of both datasets (D3).

4.1 Prediction of Vertical Land Motion

When only the vertical land motion rates are incorporated into the prior model in the D1 scenario, the peak predicted vertical uplift rate is 14.7 mm/yr to the southeast of Hudson Bay (Figure 4a). West of Hudson Bay, a smaller secondary dome of uplift is predicted, with a maximum uplift rate of 11.3 mm/yr. The estimated 2σ rates of the predictions range from ~0.6-0.8 mm/yr in more southern portions of the study area to 0.8-2 mm/yr in more northern regions of the study area (Figure 4d). The largest predicted 2σ rates (~2 mm/yr) occur within Hudson Bay, where there is no constraint on the rate of vertical land motion.

In the D2 scenario, the peak uplift rates southeast and west of Hudson Bay are 15.5 mm/yr, and 12.5 mm/yr, respectively (Figure 4b). Relative to D1, the D2 prediction lacks the northwest-southeast trending band of subsidence that is observed to the south of the margin of the former ice sheet (Figure 4b). For D2, the 2σ uncertainties range from 0.2 mm/yr to 1.2 mm/yr (Figure 4e). When both datasets are incorporated in the D3 scenario, the peak uplift rates east and west of Hudson Bay are 15.0 mm/yr and 11.2 mm/yr, respectively (Figure 4c). The predicted vertical motion uncertainty rates for D3 are between 0.2-0.6 mm/yr in the southern part of the study area, 0.6-1.2 mm/yr in the northern part of the study area, and peak in Hudson Bay (Figure 4f).

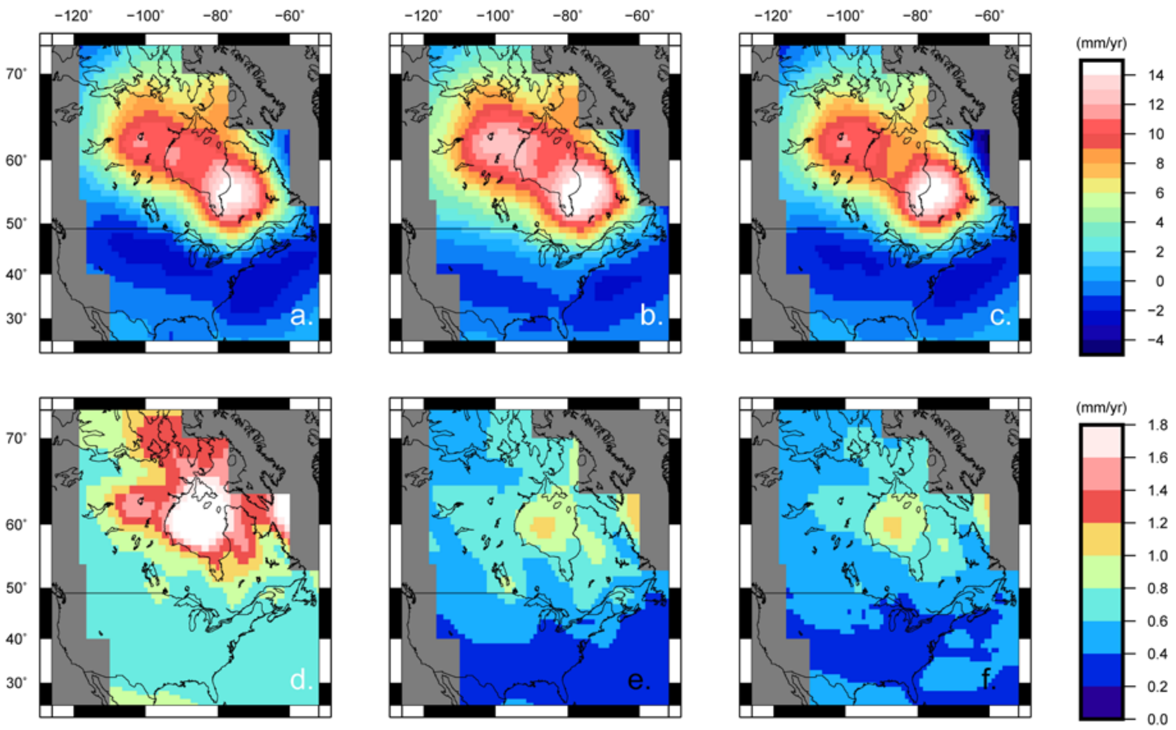

Figure 4. Results for prediction of rates of GIA-induced vertical land motion for three scenarios: a) inversion of the vertical motion data only (D1), b) inversion of the gravity change data only (D2), and c) inversion of both the vertical motion and gravity data (D3). (d-f) the predicted posterior 2σ uncertainties for each of (a-c). Uncertainties are not VCE scaled.

4.2 Prediction of Gravity Change

In general, the model predictions of gravity change are analogous to those for vertical motion (Figure 5). All scenarios predict two distinct positive anomalies in the gravity trend west and east of Hudson Bay, and in all cases, the peak rate of the eastern anomaly is predicted to be somewhat larger than the western anomaly. The respective eastern and western peak rates for the combined D3 solution are 58 mm/yr and 44 mm/yr of change in equivalent water layer thickness (EWLT). For D3, the 2σ uncertainties range from approximately 3-4 mm/yr EWLT. The most prominent difference between the three model predictions is in the region around the southern boundary of the former Laurentide Ice Sheet. Here, as with the vertical motion predictions, inclusion of the GPS data in models D1 and D3 decreases the model-predicted gravity signal, and in the case of D1, a band of negative values is predicted that is not present in the GRACE data.

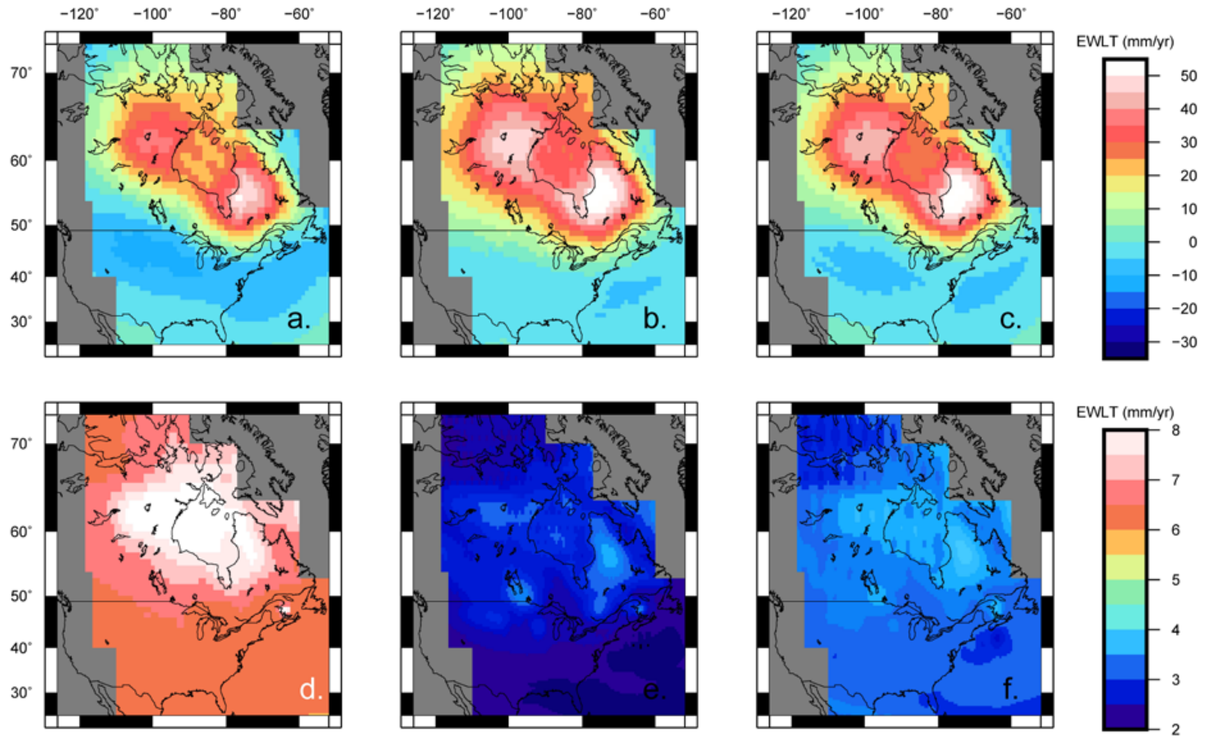

Figure 5. Results for prediction of rates of GIA-induced gravity change for three scenarios: a) inversion of the vertical motion data only (D1), b) inversion of the gravity change data only (D2), and c) inversion of both the vertical motion and gravity data (D3). (d-f) the predicted posterior 2σ uncertainties for each of (a-c). Shown in mm/yr of change to equivalent water layer thickness. Uncertainties are not VCE scaled.

4.3 Results of Variance Component Estimation

Variance component estimation is used to weight the datasets relative to each other and relative to the prior model information. Following Koch and Kusche (2002), the VCE iteratively determines the weighting factors applied to each input dataset (equation 2.8). The converged variance weighting factors and their ratios are given in Table 1. The ratios describe how each input is weighted relative to the other(s) in the model solution. In D3, the prior information is down-weighted by a factor of 1.1, and the gravity data are weighted relative to the vertical motion data by a factor of ~0.13. The gravity data are therefore weighted less heavily than the vertical motion data in the D3 solution; however, adding the gravity data significantly improves the fit of the model-predicted gravity rates to the observations (next section). In general, the predicted solutions with and without VCE are quite similar, although down-weighting of the prior information moderately increases the predicted model uncertainties (see supplementary material).

5. Discussion

5.1 Evaluation of the Predicted Models: RMS Misfits and Post-fit Residuals

Table 2 summarizes the RMS misfits between the datasets and the different model scenarios. When only the vertical data are incorporated in the D1 scenario, the RMS misfit is 1.06 mm/yr. Not surprisingly, the poorest fit to the vertical motion observations occurs when only the gravity data are incorporated in the model (RMS = 2.06 mm/yr). The poorer fit of D2 to the vertical motion data is in part due to the lack of prediction of the northwest-southeast trending band of subsidence observed near the southern margin of the former ice sheet, which is likely due to the GIA effect of a collapsing peripheral bulge in the mantle. There is no analogous signal present in the gravity data, which may indicate either a limit to the spatial resolution of the GRACE data, or that the effect of mass redistribution on gravity is small relative to its direct effect on vertical motion. D3's RMS value for prediction of vertical motion is 1.25 mm/yr.

Incorporation of only the vertical motion data provides the poorest fit to the gravity data (RMS = 1.24 mm/yr). As expected, the best-fit to the gravity change observations occurs when the gravity data are incorporated in the prior model (RMS = 0.57, and 0.76 mm/yr for D2 and D3, respectively). The combined D3 model provides the best overall prediction of both vertical motion and gravity change (Table 2).

We also calculate the corresponding RMS and χ^2 misfit values of the recent ICE-6G forward model (Peltier et al. 2015). Relative to the vertical land motion and gravity change data, ICE-6G's respective RMS values are 1.52 and 0.96 mm/yr (Table 2). The equivalent χ^2 values are 1.3 and 15.7, which yields a total χ^2 value of 9.6 and indicates that the misfits to the GRACE data are largest in regions where the error is lowest (i.e., the north). The reasonable fit (both RMS and χ^2) of ICE-6G to the vertical motion data is expected since these data were used to constrain the model. GRACE gravity data, in contrast, were not used to constrain ICE-6G, but rather used as an independent dataset for comparison with model predictions. In their own comparison, Peltier et al. (2015) noted further improvement of ICE-6G's fit to the gravity data may require modifications to the hydrology correction or to ICE-6G itself. The RMS misfit values for ICE-6G are most similar to those of the D1 model, which uses only the vertical land motion data as observational constraint.

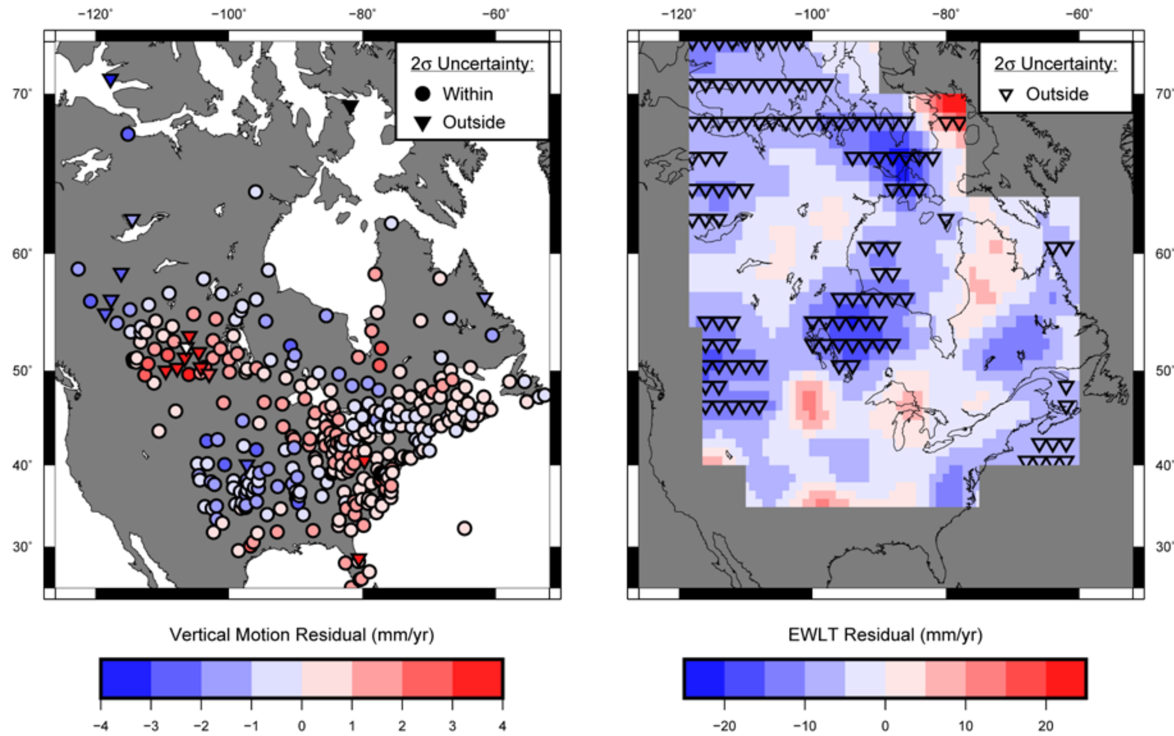

Figure 6. Residuals of model predictions relative to observations for vertical motion (left) and gravity change (right). Residuals that are within the 2σ uncertainty of the observations are plotted with a circle (left only); residuals that exceed the 2σ uncertainty of the observations are plotted with an inverted triangle (left and right). Model prediction is for the D3 combined data scenario (both vertical motion and gravity change data are incorporated).

The individual post-fit residuals provide an additional evaluation of model fit (Figure 6). For most sites within the study region, the D3 model predicts rates of vertical motion within the uncertainty of the observations. However, there is a notable region of misfit centred on approximately 110° W (west of Lake Winnipeg, Figure 1) where the model overpredicts the rate of vertical motion relative to the data

(Figure 6a). Comparison of ICE-6G predictions to vertical motion observations shows a similar misfit in this region (e.g., Snay et al. 2016). The rates of gravity change predicted by D3 are also within the data uncertainties for large parts of the study area, with coherent regions of misfit remaining west of Lake Winnipeg, southwest of Hudson Bay, and in the northern part of the model domain (Figure 6b).

These regions of misfit may be partly explained by missing or inaccurate representation of non-GIA processes within the model inputs. The separation approaches of both Lambert et al. (2013) and Wang et al. (2013, 2015) indicate a large increase in water storage after 2005 in the upper Assiniboine River watershed of the Canadian prairies west of Lake Winnipeg, an inference further supported by in-situ hydrological measurements. These studies estimate that water accumulation in this region yields a positive mass anomaly of between 20-34 mm/yr EWLT. This anomaly is not present in PCR-GLOBWB (Figure 2b), and its location approximately corresponds with a region of significant misfit in our gravity predictions (Figure 6b). Because the model underpredicts the gravity signal around Lake Winnipeg, removal of a positive hydrological anomaly in this region may improve the fit of the model to the data. Underprediction of the gravity signal by the model in the northern part of the study area may similarly indicate modification to the hydrology model is needed in this region, as well as unmodelled influences from mass loss of nearby glaciers (Figure 2b). The prediction of vertical motion will likewise be affected by any unmodelled hydrology signals, although the correction for hydrological changes is smaller for vertical motion data than it is for gravity change measurements (Section 3.3). West of Lake Winnipeg, vertical land motion data may also be influenced by pronounced localized subsidence caused by extensive potash mining in southern Saskatchewan (Samsonov et al. 2014), an effect not considered prior to inversion of the data. Further effort to identify and remove any remaining non-GIA signals from the vertical motion data may be needed to reconcile the GIA model with the data in this region (Figure 6a). Use of PCR-GLOBWB, however, improves the fit of the D3 model prediction to vertical motion observations west and east of Hudson Bay.

5.2 Predicted GIA Uncertainty

Because many studies use forward GIA models for a variety of applications, it is useful to have some measure of the uncertainty associated with GIA predictions. GIA uncertainty estimates generated by variation of forward model parameters tend to provide only broad constraint, as the variation in rates is often of the same order of magnitude as the predicted signal (Figures 3b,d). The method presented here provides an alternative means of estimating the uncertainty associated with the GIA process. An important assumption implicit in this discussion of the posterior uncertainty is that the input data are attributable to the GIA process only. As discussed in Section 5.1, analysis of the post-fit residuals has identified specific regions where this assumption may not hold. However, in general, the posterior uncertainty prediction quantifies how well we can expect to resolve the GIA signal, given the input data constraints and prior information. For example, when only vertical motion data are inverted, we can expect to predict GIA-induced vertical motion to within 0.6-0.8 mm/yr in the southern part of the study area where GPS sites are spatially dense and are often characterized by relatively small uncertainties (Figure 4d). The same example indicates an uncertainty of ~2 mm/yr associated with GIA vertical motion in and around Hudson Bay (Figure 4d); this is a logical result, since here the GPS sites are sparsely distributed and characterized by relatively large uncertainty, and the prior model information also has large uncertainty (Figure 3b). Incorporation of the gravity data lowers the maximum posterior uncertainty of the predicted vertical motion in D3 (Figure 4f). However, the spatial pattern of the uncertainty is largely unchanged for each of D1-D3 (Figures 4d-f), indicating that the prior information also contributes to the spatial characteristics of the posterior uncertainty. The results are similar for the prediction of gravity change (Figures 5d-f) with higher posterior uncertainty predicted in regions with higher uncertainty in the data and/or the prior information. Incorporation of the regularly gridded gravity data reduces the predicted model uncertainty (Figures 5e,f) relative to the scenario in which only vertical motion data are inverted (Figure 5d). Throughout the study area, the uncertainty associated with GIA-induced gravity change is ~3-4 mm/yr EWLT for the D3 model (Figure 5f).

5.3 A priori GIA information

The incorporation of prior GIA model information into the model solution introduces dependence of the final prediction on uncertain forward model information. The use, however, of *a priori* information permits prediction of the GIA response everywhere including in regions of poor data coverage, and provides a numerical way to relate vertical crustal motion to gravity change (i.e., vertical motion data can be used to predict gravity change, and vice versa, through their relationship in the model covariance matrix, C_m). The use of prior GIA model information may also help to identify any significant and spatially coherent non-GIA features that remain in the datasets. For example, the vertical motion data show a region of subsidence west of Lake Winnipeg, centred on approximately 110° W longitude and surrounded by larger uplift rates to the east and northwest (Figure 1). This feature is likely not GIA-induced (at least, it is unlikely that this pattern of deformation would arise from any of the forward model combinations assumed here), and it subsequently appears as a high misfit region in the final model prediction (Figure 6a), suggesting the need to account for an additional process here (Section 5.1). At minimum, this result is informative in the sense that we actually do not wish our final GIA model to succeed in the prediction of non-GIA features.

The supplementary material examines the influence of the prior information on the predicted solution. We consider three representations for the prior information in which the set of Earth models remains the same but is coupled to each of ICE-5G only, Laur16/SJD15 only, and both ice sheet histories together. Results show that the final prediction can indeed be affected by the choice of prior ice sheet history, particularly when ICE-5G is the only ice sheet history used (Figures S6-S11). This issue, however, can be largely mitigated by either the use of more data or the use of other ice histories in the prior information. We find that similar model predictions are achieved as long as either: i) sufficiently large datasets are used, or ii) sufficient variation is included in the prior Earth model and ice sheet combinations. The second point may be particularly important for study areas where constraint on the size and geometry of the past ice sheet is limited.

Although the model solution is only weakly sensitive to variations in the prior input, it is still possible that simplifications in the suite of Earth models may influence the results. Within the Earth model set, a two-layer mantle viscosity profile is varied, although mantle viscosity profiles employed in forward GIA studies often have three or more layers (e.g., Peltier et al. 2015). A narrower viscosity range than that employed would be more consistent with the VM2/VM5a viscosity profiles to which the ice sheet histories were tuned and may be more realistic, but would not capture the wider range of possible GIA deformation, including variations due to potentially heterogeneous Earth structure. As is, the constructed covariance matrix may contain a few very end-member forward models; however, the overall behaviour of the model set as a whole provides misfits consistently centred around zero (see also Section S4 in the supplementary material). Tests performed with a narrower range of upper and lower mantle viscosities predict modestly lower posterior uncertainties and create little change to the predicted signal. Studies have also suggested that the effective elastic thickness of the lithosphere in cratonic areas of North America may be ≥140 km (Zhao 2013, Tesauro et al. 2015). This value is significantly larger than the effective elastic thickness of 90 km that is used in the suite of *a priori* Earth models. Exploring the effect of variations in elastic lithospheric thickness and the use of more complex mantle viscosity profiles in the construction of the model covariance matrix may be a worthwhile future contribution to this work.

5.4 Comparison with rates from late Holocene RSL data

Finally, we evaluate the ability of the D3 GIA model to reproduce independent estimates of vertical land motion. Using relative sea-level (RSL) data from Simon et al. (2016), late Holocene rates of vertical motion are estimated at 8 locations in the northern part of the study area (Figure 7). The RSL data consist of ages and elevations of radiocarbon-dated material, including shells, bones and plant material. First, RSL change rates are calculated for each site by fitting a linear trend to RSL indicators from the last 4 kyr. Vertical motion rates are subsequently determined by adding an estimate of the contemporary geoid change rate. Over a time period of 4 kyr, relative sea level change can be considered to be largely insensitive to shorter term forcing; the rates thus provide reasonable site-specific proxies for contemporary vertical land motion associated with GIA. With the exception of Igloolik, which is near the northern boundary of our study area, the fit is satisfactory between vertical land motion rates predicted by D3 and the independent vertical rates estimated from the RSL data (Figure 7). The D3 model strongly underpredicts vertical land motion at Igloolik, likely due to both inadequate constraint in the input data and the site's relative proximity to large glaciers on Baffin Island. A linear fit may somewhat overestimate the rate of vertical motion due to the non-linear nature of GIA. This will be particularly true for time spans beyond 4 kyr and in load-central regions. However, the selected data are not strongly non-linear from 4 kyr onwards, and tests with 1.5 and 2 kyr time windows yield a similarly good fit, although the geologically-derived rates have higher uncertainties due to the shorter time period. Therefore, with the exception of Igloolik, the results indicate that in general the D3 model provides a reliable prediction of the GIA signal, at least in the formerly glaciated part of the study area.

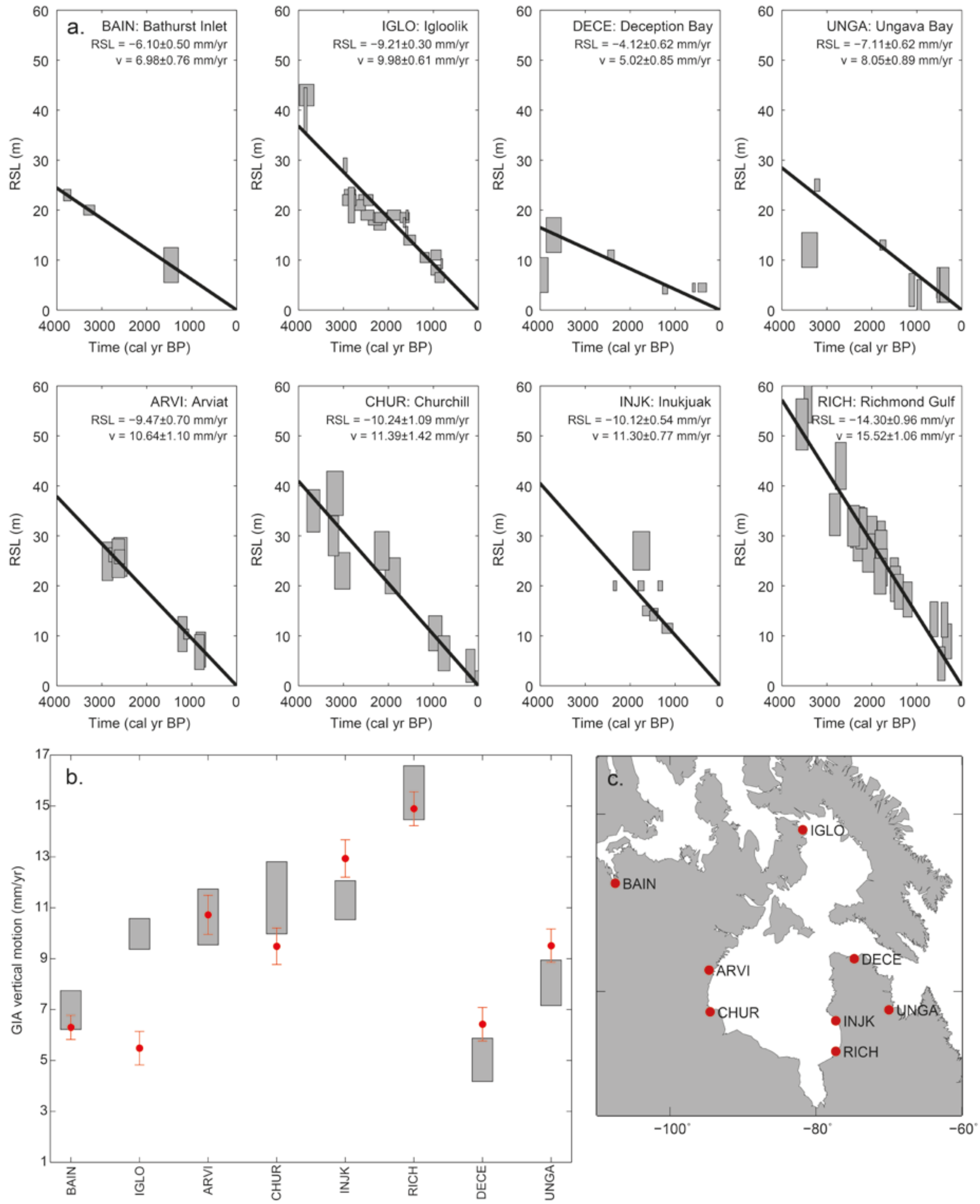

Figure 7. a) Late Holocene RSL data for 8 sites. 'RSL' gives the rate of change of relative sea level derived from a linear fit (black line), 'v' gives the associated rate of vertical motion after addition of a term for the geoid rate of change (see text). b) Comparison of model-predicted GIA vertical motion for model D3 (red circles) with the independent estimates derived from the sea level data (grey boxes). c) Map of site locations.

6. Conclusions

We generate a data-driven prediction of the present-day GIA response in North America through the simultaneous inversion of GPS-measured vertical land motion rates, GRACE-measured gravity change rates, and *a priori* GIA model information. Our methodology expands on that of Hill et al. (2010), and includes statistically appropriate weighting of the inputs via variance component estimation. In models D1-D3, we compare the predicted results for the inversion of the vertical motion data, the gravity data, and both datasets. There are two main differences between the scenarios: i) in the RMS sense, the vertical motion data alone have the poorest ability to predict gravity change, and vice versa, and ii) inversion of the gravity dataset, with its regular grid and smaller uncertainties relative to the vertical motion data, serves to reduce the maximum posterior uncertainty of the predicted model in the northern part of the study area where GPS coverage is less dense. All scenarios show the robust prediction of two centres of uplift and mass gain to the west and east of Hudson Bay. Predictions of the D3 model provide the best overall fit to both datasets, with respective RMS misfits to the vertical and gravity change data of 1.25 mm/yr and 0.76 mm/yr EWLT.

An important assumption implicit to the methodology is that the input data arise only from the GIA process. Realization of this assumption is encouraged by correction for hydrological changes in both datasets, as well as by the exclusion of particular data points where non-GIA contributions are expected to be large. However, remaining vertical motion and gravity change misfits in D3 may be partially explained by significant non-GIA signals still present in the data, including unmodelled hydrological changes in the central Prairies west of Lake Winnipeg (Lambert et al. 2013, Wang et al. 2013, 2015), and possibly unmodelled regional vertical motion changes due to active mining (Samsonov et al. 2014). Further effort to clearly identify such features and determine their appropriate treatment (i.e., their incorporation into an *a priori* correction, or simply their removal from the input dataset) is needed. Aside from these regions of misfit, the overall agreement between model predictions and observations is very good (Figure 6); the D3 model predicts rates of vertical motion and gravity change that are within the 2σ uncertainty of the observations throughout much of the study area. When compared to the predictions of the independent ICE-6G forward model, D3 performs quite well; D3's prediction of vertical motion is slightly better (RMS = 1.25 mm/yr) but still comparable to that of ICE-6G (RMS = 1.52 mm/yr), and the prediction of gravity change is improved (RMS = 0.76 versus RMS = 0.96 mm/yr EWLT) (Table 2).

At present, the inability to quantify the long-term GIA signal accurately is a significant obstacle to achieving a comprehensive understanding of how shorter time-scale processes (e.g., ice mass loss, continental hydrology variations, etc.) contribute to present-day rates of crustal deformation, gravity change, and sea-level variation, and how these contributions may change over time. GIA uncertainty estimates generated through the variation of ice sheet and Earth rheology parameters offer little additional constraint, as these estimates are often of the same order of magnitude as the predicted signal. While a data-driven model of the kind presented here has limited ability to constrain ice/Earth model combinations, an advantage to the approach in this study is the ability to estimate the formal uncertainty of the present-day GIA response at magnitudes that are significantly smaller than the *a priori* uncertainty estimates yielded by forward modelling. The results, therefore, provide future work with a useful basis from which to constrain better non-GIA contributions to present-day rates of change.

Acknowledgements

We would like to thank Yoshihide Wada for making the PCR-GLOBWB hydrology model available and Hassan Hashemi Farahani for assistance with the GRACE data post-processing. We thank also three anonymous reviewers for comments and suggestions that improved the manuscript. This work is part of the project for a Multi-Scale Sea-Level model (MuSSeL), funded by the Netherlands Organization for Scientific Research, VIDI Grant no 864.12.012.

References

Altamimi, Z., Collilieux, X., and Métivier, L., 2011. ITRF2008: an improved solution of the international terrestrial reference frame. Journal of Geodesy 85, 457–473, doi:10.1007/s00190-011-0444-4.

Arendt, A.A., Echelmeyer, K.A., Harrison, W.D., Lingle, C.S., and Valentine, V.B., 2002. Rapid wastage of Alaska glaciers and their contribution to rising sea level. Science 297, 382-386, doi:10.1126/science.1072497.

Argus, D.F., and Peltier, W.R., 2010. Constraining models of postglacial rebound using space geodesy: a detailed assessment of model ICE-5G (VM2) and its relatives. Geophysical Journal International 181, 697-723.

Argus, D.F., Peltier, W.R., Drummond, R., and Moore, A.W., 2014. The Antarctica component of postglacial rebound model ICE-6G_C (VM5a) based on GPS positioning, exposure age dating of ice thicknesses, and relative sea level histories. Geophysical Journal International 198, 537–563, doi:10.1093/gji/ggu140.

Cheng, M.K., Tapley, B.D., and Ries, J.C., 2013. Deceleration in the Earth's oblateness. Journal of Geophysical Research 118, 740-747, doi:10.1002/jgrb.50058.

Clague, J., Harper, J.R., Hebda, R.J., and Howes, D.E., 1982. Late Quaternary sea levels and crustal movements, coastal British Columbia. Canadian Journal of Earth Sciences 19, 597-681, doi:10.1139/e82-048.

Clark, J.A., Farrell, W.E., and Peltier, W.R., 1978. Global changes in postglacial sea level: a numerical calculation. Quaternary Research 9, 265-287.

Dziewonski, A.M., and Anderson, D.L., 1981. Preliminary reference Earth model. Physics of the Earth and Planetary Interiors 25, 297-356.

Farrell, W.E., and Clark, J.A., 1976. On postglacial sea level. Geophysical Journal of the Royal Astronomical Society 46, 647-667.

Gardner, A.S., Moholdt, G., Wouters, B., Wolken, G.J., Burgess, D.O., Sharp, M.J., Cogley, J.G., Braun, C., and Labine, C., 2011. Sharply increased mass loss from glaciers and ice caps in the Canadian Arctic Archipelago. Nature 473, 357-360, doi:10.1038/nature10089.

Gunter, B.C., Didova, O., Riva, R.E.M., Ligtenberg, S.R.M., Lenaerts, J.T.M., King, M.A., van den Broeke, M.R., and Urban, T., 2014. Empirical estimation of present-day Antarctic glacial isostatic adjustment and ice mass change. The Cryosphere 8, 743–760, doi:10.5194/tc-8-743-2014.

Hill, E.M., Davis, J.L., Tamisiea, M.E., and Lidberg, M., 2010. Combination of geodetic observations and models for glacial isostatic adjustment fields in Fennoscandia. Journal of Geophysical Research 115, doi:10.1029/2009JB006967.

Ivins, E.R., Dokka, R.K., and Blom, R.G., 2007. Post-glacial sediment load and subsidence in coastal Louisiana, Geophysical Research Letters 34, doi:10.1029/2007GL030003.

Jacob, T., Wahr, J., Pfeffer, W.T., and Swenson, S., 2012. Recent contributions of glaciers and ice caps to sea level rise. Nature 482, 514-518, doi:10.1038/nature10847.

James, T., Gowan, E.J., Hutchinson, I., Clague, J.J., Barrie, J.V., and Conway, K.W., 2009a. Sea-level change and paleogeographic reconstructions, southern Vancouver Island, British Columbia, Canada. Quaternary Science Reviews 28, 1200-1216, doi:10.1016/j.quascirev.2008.12.022.

James, T.S., Gowan, E.J., Wada, I., and Wang, K., 2009b. Viscosity of the asthenosphere from glacial isostatic adjustment and subduction dynamics at the northern Cascadia subduction zone, British Columbia, Canada. Journal of Geophysical Research 114, doi:10.1029/2008JB006077.

Klees, R., Revtova, E.A., Gunter, B.C., Ditmar, P., Oudman, E., Winsemius, H.C., and Savenije, H.H.G., 2008. The design of an optimal filter for monthly GRACE gravity models. Geophysical Journal International 175, 417–432, doi:10.1111/j.1365-246X.2008.03922.x.

Koch, K.-R., and Kusche, J., 2002. Regularization of geopotential determination from satellite data by variance components. Journal of Geodesy 76, 259-268, doi:10.1007/s00190-002-0245-x.

Kolker, A.S., Allison, M.A., and Hameed, S., 2011. An evaluation of subsidence rates and sea-level variability in the northern Gulf of Mexico. Geophysical Research Letters 38, doi:10.1029/2011GL049458.

Lambeck, K., Smither, C., and Johnston, P., 1998. Sea-level change, glacial rebound and mantle viscosity for northern Europe. Geophysical Journal International 134, 102–144.

Lambert, A., Courtier, N., and James, T.S., 2006. Long-term monitoring by absolute gravimetry: Tides to postglacial rebound. Journal of Geodynamics 41, 307–317, doi:10.1016/j.jog.2005.08.032.

Lambert, A., Huang, J., van der Kamp, G., Henton, J., Mazzotti, S., James, T.S., Courtier, N., and Barr, A.G., 2013. Measuring water accumulation rates using GRACE data in areas experiencing glacial isostatic adjustment: The Nelson River basin. Geophysical Research Letters 40, 6118–6122, doi:10.1002/2013GL057973.

Latychev, K., Mitrovica, J.X., Tamisiea, M.E., Tromp, J., and Moucha, R., 2005. Influence of lithospheric thickness variations on 3-D crustal velocities due to glacial isostatic adjustment. Geophysical Research Letters 32, doi:10.1029/2004GL021454.

Letetrel, C., Karpytchev, M., Bouin, M.-N., Marcos, M., Santamaría-Gómez, A., and Wöppelmann, G., 2015. Estimation of vertical land movement rates along the coasts of the Gulf of Mexico over the past decades. Continental Shelf Research 111, 42–51, doi:10.1016/j.csr.2015.10.018.

Mitrovica, J.X., and Peltier, W.R., 1991. On postglacial geoid subsidence over the equatorial oceans. Journal of Geophysical Research 96, 20,053-20,071.

Mitrovica, J.X., and Davis, J.L., 1995. Present-day post-glacial sea level change far from the Late Pleistocene ice sheets: Implications for recent analyses of tide gauge records. Geophysical Research Letters 22, 2529-2532.

Peltier, W.R., 1974. The impulse response of a Maxwell Earth. Reviews of Geophysics and Space Physics 12, 649-669.

Peltier, W.R., and Andrews, J.T., 1976. Glacial-isostatic adjustment I – The forward problem. Geophysical Journal of the Royal Astronomical Society 46, 605-646.

Peltier, W.R. and Tushingham, A.M., 1989. Global sea level rise and the greenhouse effect: might they be connected? Science 244, 806-810, doi:10.1126/science.244.4906.806.

Peltier, W.R., 2004. Global glacial isostasy and the surface of the ice-age Earth: The ICE-5G (VM2) model and GRACE. Annual Reviews of Earth and Planetary Sciences 32, 111–149, doi:10.1146/annurev.earth.32.082503.144359.

Peltier, W.R., Argus, D.F., and Drummond, R., 2015. Space geodesy constrains ice age terminal deglaciation: The global ICE-6G_C (VM5a) model. Journal of Geophysical Research 119, doi:10.1002/2014JB011176.

Rietbroek, R., Brunnabend, S.-E., Kusche, J., and Schröter, J., 2012. Resolving sea level contributions by identifying fingerprints in time-variable gravity and altimetry. Journal of Geodynamics 59–60, 72–81, doi:10.1016/j.jog.2011.06.007.

Riva, R.E.M., Gunter, B.C., Urban, T.J., Vermeersen, B.L.A., Lindenbergh, R.C., Helsen, M.M., Bamber, J.L., van de Wal, R.S.W., van den Broeke, M.R., and Schutz, B.E., 2009. Glacial isostatic adjustment over Antarctica from combined ICESat and GRACE satellite data. Earth and Planetary Science Letters 288 516–523, doi:10.1016/j.epsl.2009.10.013.

Roy, K., and Peltier, W.R., 2015. Glacial isostatic adjustment, relative sea level history and mantle viscosity: reconciling relative sea level model predictions for the U.S. East coast with geological constraints. Geophysical Journal International 201, 1156–1181, doi:10.1093/gji/ggv066.

Samsonov, S.V., González, P.J., Tiampo, K.F., and d'Oreye, N., 2014. Modeling of fast ground subsidence observed in southern Saskatchewan (Canada) during 2008–2011. Natural Hazards and Earth System Sciences, 14, 247–257, doi:10.5194/nhess-14-247-2014.

Sasgen, I., Klemann, V., and Martinec, Z., 2012. Towards the inversion of GRACE gravity fields for present-day ice-mass changes and glacial-isostatic adjustment in North America and Greenland. Journal of Geodynamics 59–60, 49–63, doi:10.1016/j.jog.2012.03.004.

Sasgen, I., Konrad, H., Ivins, E.R., van den Broeke, M.R., Bamber, J.L., Martinec, Z., and Klemann, V., 2013. Antarctic ice-mass balance 2003 to 2012: regional reanalysis of GRACE satellite gravimetry measurements with improved estimate of glacial-isostatic adjustment based on GPS uplift rates. The Cryosphere 7, 1499–1512, doi:10.5194/tc-7-1499-2013.

Sella, G.F., Stein, S., Dixon, T.H., Craymer, M., James, T.S., Mazzotti, S., and Dokka, R.K., 2007. Observation of glacial isostatic adjustment in 'stable' North America with GPS. Geophysical Research Letters 34, doi:10.1029/2006GL027081.

Siemes, C., Ditmar, P., Riva, R.E.M., Slobbe, D.C., Liu, X.L., and Hashemi Farahani, H., 2013. Estimation of mass change trends in the Earth's system on the basis of GRACE satellite data, with application to Greenland. Journal of Geodesy 87, 69–87, doi:10.1007/s00190-012-0580-5.

Simon, K.M., James, T.S., and Dyke, A.S., 2015. A new glacial isostatic adjustment model of the Innuitian Ice Sheet, Arctic Canada. Quaternary Science Reviews 119, 11–21, doi:10.1016/j.quascirev.2015.04.007.

Simon, K.M., James, T.S., Henton, J.A., and Dyke, A.S., 2016. A glacial isostatic adjustment model for the central and northern Laurentide Ice Sheet based on relative sea-level and GPS measurements. Geophysical Journal International, 205, 1618-1636, doi:10.1093/gji/ggw103.

Snay, R.A., Freymueller, J.T., Craymer, M.R., Pearson, C.F., and Saleh, J., 2016. Modeling 3-D crustal velocities in the United States and Canada. Journal of Geophysical Research 121, doi:10.1002/2016JB012884.

Spada, G., Antonioli, A., Cianetti, S., and Giunchi, C., 2006. Glacial isostatic adjustment and relative sea-level changes: the role of lithospheric and upper mantle heterogeneities in a 3-D spherical Earth. Geophysical Journal International 165, 692–702, doi:10.1111/j.1365-246X.2006.02969.x.

Tamisiea, M.E., 2011. Ongoing glacial isostatic contributions to observations of sea level change. Geophysical Journal International 186, 1036–1044, doi:10.1111/j.1365-246X.2011.05116.x.

Tamisiea, M.E., and Mitrovica, J.X., 2011. The moving boundaries of sea level change: Understanding the origins of geographic variability. Oceanography 24, 24–39, doi:10.5670/oceanog.2011.25.

Tarantola, A., 2005. Inverse problem theory and methods for model parameter estimation. Society for Industrial and Applied Mathematics, Philadelphia, 342 pp.

Tesauro, M., Kaban, M.K., and Mooney, W.D., 2015. Variations of the lithospheric strength and elastic thickness in North America. Geochemistry, Geophysics, Geosystems 16, doi:10.1002/2015GC005937.

Tushingham, A.M., and Peltier, W.R., 1991. Ice-3G: A new global model of late Pleistocene deglaciation based upon geophysical predictions of post-glacial relative sea level change. Journal of Geophysical Research 96, 4497-4523.

van der Wal, W., Wu, P., Wang, H., and Sideris, M., 2010. Sea levels and uplift rate from composite rheology in glacial isostatic adjustment modelling. Journal of Geodynamics 50, 38–48, doi:10.1016/j.jog.2010.01.006.

Wada, Y., van Beek, L.P.H., van Kempen, C.M., Reckman, J.W.T.M., Vasak, S., and Bierkens, M.F.P., 2010. Global depletion of groundwater resources. Geophysical Research Letters 37, doi:10.1029/2010GL044571.

Wada, Y., Wisser, D., and Bierkens, M.F.P., 2014. Global modeling of withdrawal, allocation and consumptive use of surface water and groundwater resources. Earth System Dynamics 5, 15–40, doi:10.5194/esd-5-15-2014.

Wahr, J., Han, D., and Trupin, A., 1995. Predictions of vertical uplift caused by changing polar ice volumes on a viscoelastic earth. Geophysical Research Letters 22, 977-980.

Wang, H., Jia, L., Steffen, H., Wu, P., Jiang, L., Hsu, H., Xiang, L., Wang, Z., and Hu, B., 2013. Increased water storage in North America and Scandinavia from GRACE gravity data. Nature Geoscience 6, 38-42, doi:10.1038/ngeo1652.

Wang, H., Xiang, L., Jia, L., Wu, P., Steffen, H., Jiang, L., and Shen, Q., 2015. Water storage changes in North America retrieved from GRACE gravity and GPS data. Geodesy and Geodynamics 6, 267-273, doi:10.1016/j.geog.2015.07.002.

Wu, X., Heflin, M.B., Schotman, H., Vermeersen, B.L.A., Dong, D., Gross, R.S., Ivins, E.R., Moore, A.W., and Owen, S.E., 2010a. Simultaneous estimation of global present-day water transport and glacial isostatic adjustment. Nature Geoscience 3, 642-646, doi:10.1038/ngeo938.

Wu, P., Steffen, H., and Wang, H., 2010b. Optimal locations for GPS measurements in North America and northern Europe for constraining glacial isostatic adjustment. Geophysical Journal International 181, 653–664, doi:10.1111/j.1365-246X.2010.04545.x

Zhang, Z.Z., Chao, B.F., Lu, Y., and Hsu, H.T. (2009). An effective filtering for GRACE time-variable gravity: Fan filter. Geophysical Research Letters, 36, doi: 10.1029/2009GL039459.

Zhao, S., 2013. Lithosphere thickness and mantle viscosity estimated from joint inversion of GPS and GRACE-derived radial deformation and gravity rates in North America. Geophysical Journal International 194, 1455–1472, doi:10.1093/gji/ggt212.

Tables

Data Incorporated	σ^2 Squared Value			Ratios	
	σ_1^2 (Vertical)	σ_2^2 (Gravity)	σ_μ^2 (Prior)	σ_1^2/σ_2^2	σ_1^2/σ_μ^2, σ_2^2/σ_μ^2
D1: Vertical only	1.1	-	7.1	-	0.15, -
D2: Gravity only	-	9.3	0.5	-	-, 18.6
D3: Vertical+Gravity	1.4	10.9	1.1	0.13	1.3, 9.9

Table 1. Results of the variance component analysis. $\sigma_1^2$and σ_2^2 are the variance factors applied to the vertical motion data (dataset 1) and gravity change data (dataset 2), respectively, and σ_μ^2 is the variance factor applied to the prior information. The ratios describe how each input is weighted relative to the other(s).

Model Type	**RMS Values**	
	Vertical Motion (mm/yr)	Gravity Change (mm/yr EWLT)
	Evaluation of Inputs	
Null	3.36	2.65
Prior	2.64	1.02
	Data-Driven Inversion	
D1: Vertical only	1.06	1.24
D2: Gravity only	2.06	0.57
D3: Vertical+Gravity	1.25	0.76
	Forward GIA Model Comparison	
ICE-6G	1.52	0.82

Table 2. RMS values of model predictions relative to observations for vertical crustal motion and gravity change. Null model gives the RMS value of the data set relative to no model prediction, and prior model gives the RMS of the *a priori* average model relative to the observations. Data-driven model results shown for three input data scenarios: vertical land motion data ('Vertical only', D1), gravity change observations ('Gravity only', D2) and both datasets ('Vertical+Gravity', D3). Vertical motion RMS values calculated for n_{gps} = 340 sites; gravity change RMS values calculated for n_{grace} = 468 sites. Units for vertical and gravity change are mm/yr and mm/yr of EWLT change, respectively.